

# Sub-quadratic scalable approximate linear converter using multi-plane light conversion with low-entropy mode mixers

Yoshitaka Taguchi<sup>1,\*</sup>

<sup>1</sup>*Department of Electrical Engineering and Information Systems,  
The University of Tokyo, 7-3-1 Hongo, Bunkyo-ku, Tokyo 113-8656 Japan*

(Dated: December 17, 2024)

Optical computing is emerging as a promising platform for energy-efficient, high-throughput hardware in deep learning. A key challenge lies in the realization of optical matrix-vector multiplication, which often requires  $O(N^2)$  phase shifters for exact synthesis of  $N \times N$  matrices, limiting scalability. In this study, we propose an approximate matrix realization method using multi-plane light conversion (MPLC) that reduces both the system size and the number of phase shifters while maintaining acceptable error bounds. This approach uses low-entropy mode mixers, allowing more compact implementations compared to conventional mixers. We introduce Shannon matrix entropy as a measure of mode coupling strength in mixers and demonstrate that low-entropy mixers can preserve computational accuracy while reducing the requirements for the mixers. The approximation quality is evaluated using the maximum norm between the target and realized matrices. Numerical results show that the proposed method achieves sub-quadratic scaling of phase shifters by tolerating predefined error thresholds. To identify efficient architectures for implementing general linear matrices, we compare block-encoding (BE) and singular-value decomposition (SVD) schemes for realizing general linear matrices using unitary converters based on MPLC. Results indicate that BE exhibits superior iterative configuration properties beyond the unitary group. By characterizing the trade-offs between matrix entropy, number of phase shifter layers, and the error tolerance, this study provides a framework for designing scalable and efficient approximate optical converters.

## I. INTRODUCTION

Optical computing is emerging as a promising hardware platform for energy-efficient and high-throughput computing [1–10]. As modern deep learning models increasingly rely on architectures with a large number of parameters, scalability on photonic platforms has gained attention [11–14]. A major challenge in this area is the increasing number of components and the growing system size. Phase-shifter-based photonic circuits can achieve arbitrary unitary transformations using  $O(N^2)$  phase shifters. Real-valued matrices, commonly used in deep learning models, can be realized through unitary matrices using techniques such as singular value decomposition (SVD) [1, 15] or block encoding (BE) [16, 17]. On integrated photonics platforms, cross-bar array wiring of thermo-optic phase shifters [18, 19] and phase-change-material-based modulators [20–22] can reduce the number of wires required. While this approach achieves  $O(N)$  scaling in terms of wiring, the low operational speed of these modulators limits their practical applications. Alternatively, wavelength multiplexing parallelizes the calculation to reduce the system size [23–25], but quadratic scaling challenges remain. Another approach involves training models directly on photonic platforms with smaller number of components, embedding the physical system’s properties into the model itself [26–29]. However, this strategy requires training models from scratch, or additional training of the pre-trained

models developed on GPUs. This limits the reuse of existing machine learning assets.

On conventional semiconductor-based computing platforms, model quantization is a widely adopted technique for efficient inference. Quantization of model weights, which represents weight values using fewer bits, reduces both the complexity of semiconductor circuits in computing units and memory requirements [30–33]. During quantization, weights are converted to integer representations, introducing quantization errors into the model. Extensive research has been conducted to address these errors, enabling quantized models to achieve performance comparable to their original counterparts. Remarkably, even models with weights represented using only a few bits can maintain high performance [34–36]. While these approximation techniques are widely implemented, they have yet to be extensively studied in the context of optical computing. Given that optical computing is inherently analog, adopting proactive approximation methods could capitalize on its unique computational characteristics.

In this study, we propose a compact and scalable programmable linear converter based on multi-plane light conversion (MPLC) [37–39] for approximate computation. The MPLC architecture has demonstrated its capability to implement both target unitary transformations and real-valued linear conversions. While prior research has established exact configuration methods for MPLC architectures [40–43], their potential for approximate computation remains unexplored. Here, we investigate the approximation capabilities of MPLC by analyzing the effects of varying the entropy of mode mixers and the number of phase-shifter layers. Shannon entropy is employed as a metric for mode mixing, providing a quan-

---

\* yoshi.taguchi@alumni.u-tokyo.ac.jp

titative measure of how effectively a linear transformation mixes different modes. Previous research has shown that the MPLC architecture using mode mixers with low entropy can be universally configurable [44–46]; however, the quantitative relationship between matrix entropy and approximation accuracy remains unexplored. Our findings reveal that the relationship between entropy and error exhibits a plateau, indicating that MPLC architectures can be designed with low-entropy mode mixers without compromising error tolerance. By utilizing mode mixers with small entropy, it is possible to employ compact mixers, thereby reducing the overall system size. Furthermore, we demonstrate that allowing for some error in the realized matrix enables sub-quadratic scaling of the number of phase shifters, compared to the quadratic scaling required for exact synthesis. We evaluate the approximation capability by measuring the maximum element-wise error in the synthesized matrix, offering an intuitive, quantization-like assessment of accuracy. The error bound is analyzed as a function of matrix entropy and the number of phase shifters or phase-shifter layers, providing design guidelines for constructing approximate linear converters within a specified error tolerance.

This paper is organized as follows. In Section II, we begin by discussing the fundamental properties of Shannon matrix entropy in relation to unitaries and mode mixing. We introduce a matrix interpolation between a given matrix and the identity matrix within the unitary group, providing a method for sampling unitary matrices with a specified Shannon entropy. We statistically investigate the relationship between entropy and mode mixing, offering an intuitive interpretation of Shannon entropy. In Section III, we examine the exact synthesis of unitary matrices and general matrices using the MPLC architecture. First, we demonstrate that even with low-entropy mode mixers, a few-redundant MPLC architecture can be configured to achieve a target unitary matrix. The accuracy of matrix realization depends monotonically on the matrix entropy of the mode mixers. These results indicate that Shannon matrix entropy serves as a critical metric for designing mode mixers in MPLC architectures. Second, we address the synthesis of general matrices and show that the BE scheme is advantageous over the SVD scheme in terms of configuration efficiency and the number of required phase shifters. We also provide an algebraic proof of the minimum number of layers necessary for universal synthesis using the BE scheme. Section IV examines approximate converters based on MPLC architectures with an insufficient number of layers. While these converters cannot achieve exact synthesis, the number of required phase shifters scales sub-quadratically with the matrix size  $N$ , given a tolerable error bound. We systematically evaluate approximation errors by varying the number of phase-shifter layers and the matrix entropy. Section V concludes this paper.

## II. SHANNON ENTROPY OF UNITARY MATRICES

In this section, we introduce the concept of Shannon entropy for mode mixers and outline its fundamental properties. Shannon entropy is defined for unistochastic matrices [47], which are widely studied in fields such as quantum mechanics on graphs [48–51]. A unistochastic matrix  $B$  is derived from a unitary matrix  $U$  as  $B_{ij} = |U_{ij}|^2$ . For a complex vector  $\mathbf{v}$ , each element of  $B$  represents the proportion of mixing among the components of  $\mathbf{v}$  induced by the linear transformation  $U\mathbf{v}$ . The matrix  $B$  satisfies the following conditions:

$$B_{ij} \geq 0, \quad \sum_i B_{ij} = 1, \quad \sum_j B_{ij} = 1, \quad (1)$$

resembling the properties of a discrete probability distribution for the rows and columns of  $B$ . Applying the entropy function  $-\sum p(x) \ln p(x)$  for each row of  $B$  defines the Shannon entropy for a unistochastic matrix  $B$  [52]:

$$-\frac{1}{N} \sum_{ij} B_{ij} \ln B_{ij}, \quad (2)$$

where  $N$  is the matrix size. The Shannon entropy ranges between its minimum value of 0 and maximum value of  $\ln N$  [53]. In this study, we define the normalized Shannon entropy for a mode mixer with a transfer matrix represented by  $U$  as:

$$\mathcal{H}(U) = -\frac{1}{N \ln N} \sum_{ij} |U_{ij}|^2 \ln |U_{ij}|^2, \quad (3)$$

where the normalization by  $\ln N$  ensures that  $0 \leq \mathcal{H}(U) \leq 1$ . Unitary matrices satisfying  $\mathcal{H}(U) = 0$  correspond to permutation matrices, where each row and column contains only one nonzero entry equal to one.

We define an interpolating function  $\tau_U(\alpha) : \mathbb{R}_{\geq 0} \rightarrow U(N)$  for a given unitary matrix  $U$ :

$$\tau_U(\alpha) = U^\alpha = V^{-1} D^\alpha V, \quad (4)$$

where  $U = V^{-1} D V$  represents the diagonalization of  $U$ , and  $D^\alpha = \text{diag}(d_{11}^\alpha, d_{22}^\alpha, \dots, d_{nn}^\alpha)$ . For  $0 \leq \alpha \leq 1$ ,  $\tau_U(\alpha)$  interpolates on the unitary group between the identity matrix  $I$  and the given matrix  $U$ , satisfying  $\tau_U(0) = I$ ,  $\tau_U(1) = U$ , and  $\tau_U(\alpha) \in U(N)$ . This function can also be interpreted as the unitary time evolution of a system, since for any Hermitian matrix  $H$ , there exists a unitary matrix  $U$  such that  $\exp(iHt/\hbar) = \exp(iH/\hbar)^t = U^t$ . We investigate the behavior of Shannon entropy  $\mathcal{H}(\tau_U(\alpha))$  under this interpolation and demonstrate its monotonicity. Figure 1 presents  $\mathcal{H}(\tau_U(\alpha))$  and its derivative  $\mathcal{H}'(\tau_U(\alpha))$  as a function of  $\alpha$  for  $N = 8$  and  $N = 32$ . These values are evaluated for 64 samples of unitary matrices  $U$ . The shaded area shows the range of minimum and maximum values, the dotted line shows the 25% and

75% quantiles, and the solid line shows the median. The unitary matrix  $U$  is sampled from Haar measure using the `stats` module of SciPy. The results show that Shannon entropy monotonically increases for  $0 \leq \alpha \leq 1$  and saturates for  $1 \leq \alpha$ , similar to previous findings of von Neumann entanglement entropy in the time evolution of quantum systems [54–56]. This monotonic property is utilized throughout this paper to sample unitary matrices with a specified target entropy, i.e., sampling  $U$  such that  $\mathcal{H}(U) = t$  for given  $t$ .

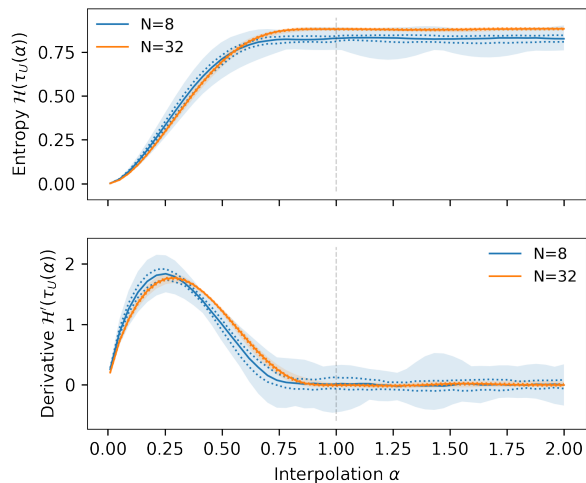


FIG. 1: Shannon matrix entropy  $\mathcal{H}(\tau_U(\alpha))$  and its derivative  $\mathcal{H}'(\tau_U(\alpha))$  as functions of the interpolation parameter  $\alpha$ . The values are computed while sampling the unitary matrix  $U$  for 64 times. The shaded area represents minimum and maximum values, the solid line represents the median, and the dotted line represents 25% and 75% quantiles of samples, respectively.

We further examine the relationship between the non-diagonal matrix elements and entropy. Figure 2 illustrates the range, quantiles, and median of the squared absolute values of non-diagonal elements,  $|X_{ij}|^2$ , for  $i \neq j$ , as a function of entropy  $h$ . For a given target entropy  $h$ , matrix  $X$  satisfying  $\mathcal{H}(X) = h$  is sampled 64 times, and the corresponding statistics are computed. The sampling process involves numerically solving the equation  $\mathcal{H}(\tau_U(\alpha)) = h$  for  $0 \leq \alpha \leq 1$ , following the initial sampling of a unitary matrix  $U$ . This equation always yields a unique solution due to the monotonic relationship shown in Fig. 1. The quantiles of the non-diagonal elements exhibit a monotonic relationship with the Shannon entropy, confirming that entropy effectively measures the degree of mixing in a given matrix.

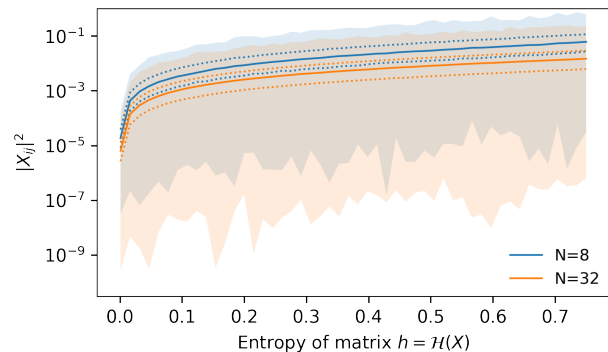


FIG. 2: Squared absolute values of non-diagonal elements for unitary matrices,  $|X_{ij}|^2$ , with  $i \neq j$ , having a specified entropy  $h = \mathcal{H}(X)$ . The 64 samples are shown in the same manner as Fig. 1.

### III. EXACT CONVERTER WITH LOW-ENTROPY MODE MIXERS

In this section, we explore the relationship between the Shannon entropy of mode mixers in the MPLC architecture and its exact configuration capabilities. Previous studies have examined the requirements for mode mixers to enable universal configuration in MPLC architectures using specific mode mixers [45, 57, 58]. Here, we focus on the configuration capabilities of MPLC architectures with mode mixers characterized by their Shannon entropy. Both the synthesis of unitary matrices and general linear matrices are analyzed. For the synthesis of general linear matrices, we compare two approaches: the SVD scheme and the BE scheme. Our results demonstrate that the entropy of mode mixers can be reduced without compromising the universality, and that the BE scheme is advantageous for iterative configuration.

#### A. Device definition

We formally define the unitary converter based on the MPLC architecture. In this paper, we use the few-layer redundant MPLC architecture [43, 58, 59]. This architecture has demonstrated its ability to be exactly configured to any target unitary using an iterative optimization method. The structure of this architecture is illustrated in Fig. 3. Each layer of the architecture consists of an  $N$ -port fixed unitary mode mixer  $A_i$  and an array of  $N$  single-mode phase shifters. The overall transformation of this device, denoted as  $X$ , is given by

$$X = L_{m+1}A_m L_m \cdots A_2 L_2 A_1 L_1, \quad (5)$$

where  $A_i$  is the transfer matrix of a  $N$ -port unitary mode mixer, and  $L_i$  is defined as  $L_i = \text{diag}(e^{i\theta_{i1}}, e^{i\theta_{i2}}, \dots, e^{i\theta_{in}})$ . In the few-layer redundant configuration, the number of layers,  $m$ , is set to  $N + 1$ .

Each distinct phase shift within the phase shifters is denoted by a real parameter variable, and all the phase shifts are collectively expressed as a vector  $\mathbf{p}$ .

To evaluate the exact and universal synthesis capability of this architecture, we fix the Shannon entropy of all mode mixers  $A_i$  to the same value. This uniform entropy setting is motivated by two considerations:

1. If the entropy of all mixers is zero (i.e., the mixers do not perform any mode mixing), the unitary converter cannot achieve universality.
2. Previous research [60, 61] has demonstrated the robustness of the MPLC architecture to imperfections in its mode mixers. Based on this robustness, if a converter is universally configurable, increasing the entropy of one mixer should not compromise the overall universality of the converter.

Therefore, by fixing the entropy equally across all mixers, we aim to determine the minimum entropy required for the architecture to be universal.

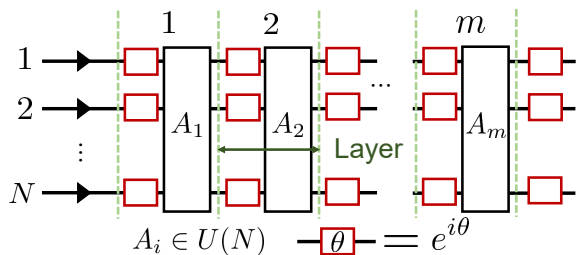


FIG. 3: Schematic representation of the  $N \times m$  MPLC architecture. The number of layers is specified by  $m$ . Each layer consists of an  $N$ -port fixed unitary converter represented by  $A_i$ , followed by an array of  $N$  single-mode phase shifters.

## B. Optimization problem setting and algorithm

The phase shifter optimization problem of exact unitary converter is formulated as follows. The normalized cost function  $\mathcal{L}$  [43] between two matrices is defined as:

$$\mathcal{L}(\mathbf{p}) = \frac{1}{4N} \|X(\mathbf{p}) - U\|_F^2, \quad (6)$$

where  $X(\mathbf{p})$  is the unitary matrix realized physically by the parameter vector  $\mathbf{p}$ ,  $U$  is the target matrix to be achieved, and  $\|\cdot\|_F$  is the Frobenius norm. To minimize  $\mathcal{L}(\mathbf{p})$ , we employ numerical optimization. At the start of the optimization, parameters are initialized using a uniform distribution ranging from 0 to  $2\pi$ , and the target unitary matrix  $U$  is sampled from the Haar measure using the `stats` module of SciPy [62]. In the MPLC architecture, each matrix  $A_i$  for  $1 \leq i \leq m$  is sampled so that the entropy of every mixer is fixed to  $h$ , that is,

$\mathcal{H}(A_i) = h$ . This entropy-fixing sampling follows the procedure outlined in Section II. After initializing the parameters and the matrix, the cost function  $\mathcal{L}$  is optimized using the quasi-Newton optimization method, specifically, the limited-memory Broyden-Fletcher-Goldfarb-Shanno (L-BFGS) algorithm [63] implemented in `optimize` module of SciPy [62]. This method starts from the initial parameters and modifies them at each step until convergence to the local minimum, where  $d\mathcal{L}/d\mathbf{p} = \mathbf{0}$ . The optimization is run 64 times while changing the initial parameters to investigate the statistical behavior. Matrices  $U$  and  $A_i$  are sampled at the each optimization. The gradient, which is essential for L-BFGS optimization algorithm, is provided by the standalone gradient method [64]. During the optimization, only information from the input and output vectors is used, and no explicit knowledge of the matrices  $A_i$  is incorporated.

## C. Synthesis of general linear using unitaries

To support broader applications, particularly in deep learning, matrix multiplication devices must be capable of handling general matrices. We assume that the matrix to be synthesized is scaled such that all its singular values are less than 1, and we refer to this matrix as a general linear matrix in this study. Two schemes for implementing general matrices using unitary matrices are considered: SVD and BE. The SVD scheme realizes a general matrix by combining a layer of intensity modulators with two unitary converters. Specifically, the matrix is decomposed into two unitary matrices and a diagonal matrix, with the diagonal matrix implemented using the intensity modulator array. The BE scheme, on the other hand, embeds the  $N \times N$  matrix into a  $2N \times 2N$  unitary matrix. This method has been used in quantum computation [65, 66], and recent research has adapted it for optical computing [16, 17].

We define the cost function for configuring a general matrix and describe how the parameter vector  $\mathbf{p}$  is mapped for the SVD and BE schemes. The cost function is based on the Frobenius norm:

$$\mathcal{L}_{\text{gen}}(\mathbf{p}) = \|Q(\mathbf{p}) - P\|_F^2, \quad (7)$$

where  $Q(\mathbf{p})$  is the matrix physically realized by the parameter vector  $\mathbf{p}$ , and  $P$  is the target matrix to be achieved. The target matrix  $P$  is generated such that its singular values are less than 1, using  $P = W_1 \text{diag}(\sigma_1, \sigma_2, \dots, \sigma_n) W_2$ , where  $W_1$  and  $W_2$  are Haar-random matrices, and the  $N$  singular values  $\sigma_i$  are sampled from the uniform distribution  $U(0, 1)$ .

In the SVD scheme,  $Q(\mathbf{p})$  is realized as:

$$Q(\mathbf{p}) = U_1(\mathbf{p}) \Sigma U_2(\mathbf{p}) \quad (8)$$

where  $U_1(\mathbf{p})$  and  $U_2(\mathbf{p})$  are unitary matrices, and  $\Sigma$  is a real diagonal matrix with elements less than 1. Half of the components in  $\mathbf{p}$  are used to parameterize  $U_1$ , and the

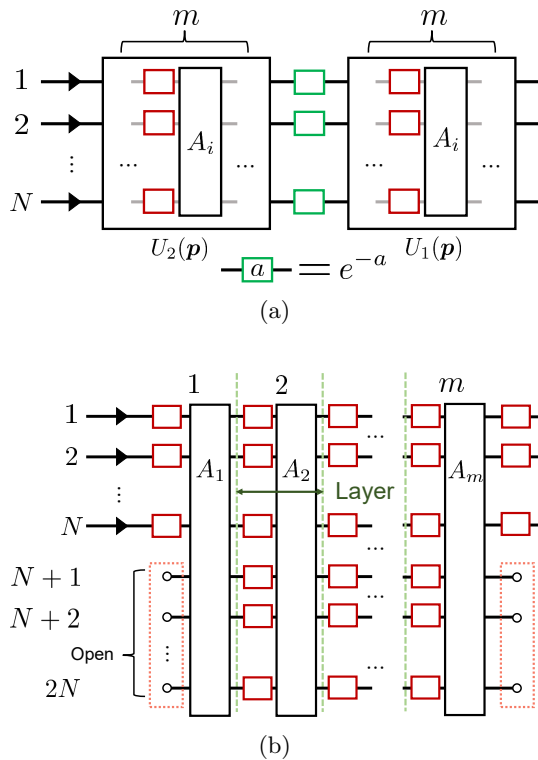


FIG. 4: Schematics of the (a) SVD and (b) BE schemes.

In the SVD scheme, the structure consists of a series connection of a unitary converter with  $m$  layers, an array of intensity modulators denoted by  $a$ , and another unitary converter with  $m$  layers. For the BE scheme, the general linear matrix is embedded into a  $2N \times 2N$  unitary matrix using an MPLC unitary converter with  $m$  layers. In this scheme,  $N$  ports are open at the input and output of the mode mixers  $A_1$  and  $A_m$ , respectively, out of the  $2N$  ports.

other half to parameterize  $U_2$ . Here, we do not include the diagonal elements of  $\Sigma$  in  $\mathbf{p}$ . This is because the total optical power at the outputs depends only on the sum of the diagonal elements of  $\Sigma$ , allowing each intensity modulator to be configured separately by measuring the total output power and adjusting the corresponding intensity. Once the intensity modulators are set, the unitary converters are configured accordingly. The standalone gradient method is used to compute the gradient  $d\mathcal{L}_{\text{gen}}/d\mathbf{p}$ , which is essential for the optimization algorithm.

In contrast, the BE scheme does not use intensity modulators and realizes a general  $N \times N$  matrix  $Q$  via the following embedding:

$$U = \begin{bmatrix} Q & \sqrt{I - QQ^\dagger} \\ \sqrt{I - Q^\dagger Q} & -Q^\dagger \end{bmatrix}, \quad (9)$$

where  $U$  is a  $2N \times 2N$  unitary matrix,  $I$  is the  $N \times N$  identity matrix, and  $\sqrt{\cdot}$  is the matrix square root. The  $2N \times 2N$  matrix  $U$  is synthesized using the MPLC architecture, with half of the input and output ports employed

to extract  $Q$ , as illustrated in Fig. 4. To determine the minimum number of layers  $m$  required to synthesize  $U$  using the MPLC architecture, we first consider the degrees of freedom in the architecture. The  $2N \times 2N$  unitary matrix  $U$  has  $(2N)^2 = 4N^2$  degrees of freedom, while the matrix square roots in the embedding Eq. 9 introduce additional unitary degree of freedom. A proof for the degree of freedom of the matrix square root is provided in the Appendix A. Since any unitary can be chosen for the matrix square root, the embedding reduces the degrees of freedom of  $U$  to  $4N^2 - 2 \times N^2 = 2N^2$ . Considering that only half of the input and output ports are used, we can disregard half the phase shifters in the first and last layers of the MPLC architecture. Denoting the number of internal layers with  $2N$  phase shifters by  $m'$ , the following inequality must hold to ensure the synthesis of  $Q$  from the perspective of degrees of freedom:

$$(N - 1) + m'(2N - 1) + (N - 1) + 1 \geq 2N^2. \quad (10)$$

Note that each phase shifter array has  $N - 1$  or  $2N - 1$  degrees of freedom due to the loss of one degree of freedom from the global phase, and the entire device has an additional degree of freedom corresponding to the global phase. Solving this inequality, noting that  $m'$  is an integer, leads to  $m' > N - 1$ . Including the first and last layers, the total number of phase shifter layers satisfies  $m' + 2 > N + 1$ , establishing that the minimum number of phase-shifter layers required is  $N + 2$ . We now conclude that the minimum number of phase-shifter layers is  $N + 2$ . This corresponds to  $m = N + 1$ , consistent with a previously proposed constructive proof [16]. However, in this work, we provide a general algebraic derivation that does not depend on specific constructions of the matrix square roots. Since the inequality in Eq. 10 does not hold as an equality for integers  $m'$ , the condition  $m = N + 1$  introduces redundancy into the system. This redundancy significantly reduces the cost function, similar to the configuration of exact unitary converter using MPLC architecture, as discussed in Sec. IIID. For the optimization, each phase shifters are collectively represented by  $\mathbf{p}$ , and the matrix  $Q(\mathbf{p})$  is obtained as the upper-left  $N \times N$  submatrix of  $U(\mathbf{p})$ . The standalone gradient method can be used to compute the exact gradient  $d\mathcal{L}_{\text{gen}}/d\mathbf{p}$  in this case as well. This is possible because the Frobenius norm over the submatrix satisfies the condition for applying the standalone gradient method, namely, that the norm varies sinusoidally with a linear sweep of the phase in each phase shifter. Similarly the optimization process for synthesizing unitaries in Sec. IIIB, only information from the input and output ports is utilized during optimization.

#### D. Results

Figure 5 shows the cost function  $\mathcal{L}$  after optimization as a function of the entropy of mode mixers for the exact unitary converter configuration. The cost function is

recorded 512 times after optimization, with the number of layers  $m$  set to  $N + 1$  for the few-redundant configuration. For both cases,  $N = 8$  and  $N = 32$ , the cost function decreases as the entropy of the mode mixers increases. Moreover, the reduction in the cost function saturates when the entropy exceeds a certain value. This indicates that mode mixers with lower entropy can be used without compromising universality, allowing the use of mode mixers with smaller footprints. For instance, in the  $N = 32$  case, mode mixers with an entropy of  $h = 0.3$  can be used without increasing the cost function  $\mathcal{L}$ . At this entropy, at least 75% of the couplings among modes in the mixers are below 1%, as shown in Fig. 2.

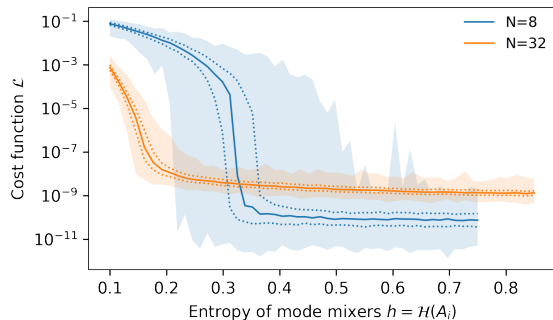


FIG. 5: Cost function  $\mathcal{L}$  as a function of entropy  $h$  for  $N = 8$  and  $N = 32$ , where all mixers  $A_i$  satisfy  $\mathcal{H}(A_i) = h$ . Results from 512 optimization are shown in the same manner as in Fig. 1.

Figure 6 shows the convergence plots comparing the SVD and BE schemes for the configuration of a general linear converter. In the SVD scheme,  $m = N$  represents the minimum number of layers required to achieve the  $N^2$  degrees of freedom in an  $N \times N$  unitary matrix. A significant shift is observed when increasing from  $m = N$  to  $m = N + 1$  in both the number of iterations required for convergence and in the final value of the cost function  $\mathcal{L}_{\text{gen}}$ , as shown in Figs. 6a and 6b. This occurs because  $m = N + 1$  corresponds to the few-redundant configuration of MPLC in each unitary converter. For BE scheme,  $m = N + 1$  is the minimum number of layers needed to provide the necessary degrees of freedom in the architecture. A substantial reduction in the cost function is observed when increasing from  $m = N$  to  $m = N + 1$ , as shown in Figs. 6c and 6d. While adding more layers significantly reduces the number of iterations, it has only a minor impact on the final cost function value. Overall, the BE scheme requires fewer iterations to converge compared to the SVD scheme and achieves a smaller final value of the cost function  $\mathcal{L}_{\text{gen}}$ . In contrast, the SVD scheme exhibits a large variance in the cost function across all cases, even though it has the sufficient number of degrees of freedom.

We further examine how the final value of the cost function changes with the number of layers in the BE scheme. Figure 7 shows the median of the final cost func-

tion  $\mathcal{L}_{\text{gen}}$  as a function of  $m/(N + 1)$ , where the median is calculated across 64 optimization trials. The number of layers  $m$  is varied from  $m = 1$  to  $m = 2N$ . For all cases ( $N = 4, 8, 16, 32$ ), a substantial decrease in the cost function is observed at  $m/(N + 1) = 1$ , corresponding to  $m = N + 1$ . This indicates that no redundant layers are needed to achieve a significant reduction in the cost function, consistent with the absence of an equality condition for the inequality in Eq. 10, as discussed in Sec III C.

#### IV. APPROXIMATE CONVERTER WITH INSUFFICIENT LAYERS

In this section, we investigate the approximation abilities of the MPLC architecture when the number of layers is insufficient. As shown in Fig. 7, the MPLC architecture retains error after optimization when the number of layers is less than the minimum required ( $m < N + 1$ ). This observation suggests that if some error in the converter can be tolerated, the number of layers in the MPLC architecture can be reduced. Our results demonstrate that for a given upper bound on the error in matrix components, the required number of phase shifters in the approximate converter scales sub-quadratically. We adopt the BE scheme for the approximate converter, as it shows better convergence performance.

To measure the error in the approximate converter, we introduce an entry-wise maximum matrix norm defined as follows:

$$\|A\|_{\max} = \max_{i,j=1,\dots,N} |A_{ij}|, \quad (11)$$

where  $A$  is a matrix. This definition is equivalent to the  $L^\infty$  norm of a vector,  $\|x\|_\infty = \max |x_i|$ , where all the matrix components are flattened and treated as elements of a vector. Since  $\|x\|_\infty$  satisfies the conditions for a norm, the matrix norm defined in Eq. 11 also satisfies the conditions. This norm represents the maximum absolute value of the matrix components, and  $\|Q(\mathbf{p}) - P\|_{\max}$  represents the maximum absolute error between the target matrix  $P$  and the realized matrix  $Q(\mathbf{p})$ . By introducing this norm, we can analyze the approximation ability of the matrix in the context of quantization techniques used in deep learning models.

##### A. Optimization problem setting and evaluation

Instead of directly minimizing  $\|\cdot\|_{\max}$ , we use the cost function  $\mathcal{L}_{\text{gen}}$  defined in Eq. 7 for the optimization of the approximate converter. This is motivated by the fact that the derivative of  $\|\cdot\|_{\max}$  cannot be explicitly expressed and is not efficiently minimized, as no convenient formulation showing its convexity is known to the best of our knowledge. However, since  $\mathcal{L}_{\text{gen}}(\mathbf{p}) = 0 \Leftrightarrow \|Q(\mathbf{p}) - P\|_{\max} = 0$ , minimizing  $\mathcal{L}_{\text{gen}}(\mathbf{p})$  is expected to



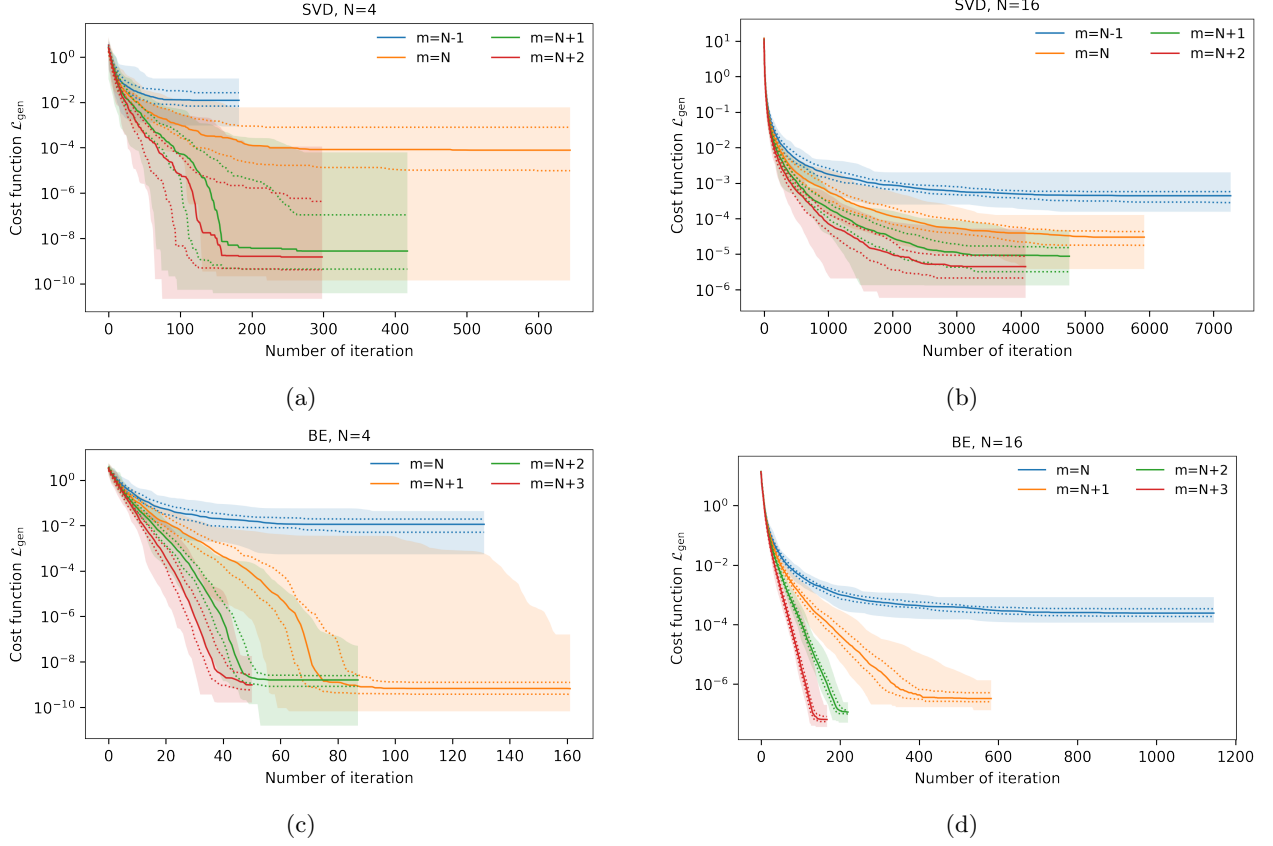


FIG. 6: Convergence plots for SVD and BE schemes. The vertical axis shows the value of the cost function  $\mathcal{L}_{\text{gen}}$  defined by Eq. 7, and the horizontal axis shows the number of iterations. The shaded area represents the minimum and maximum values, the solid line represents the median, and the dotted line represents the 25% and 75% quantiles over 64 optimization trials. SVD with (a)  $N = 4$ , (b)  $N = 8$ , BE with (c)  $N = 4$ , and (d)  $N = 16$ .

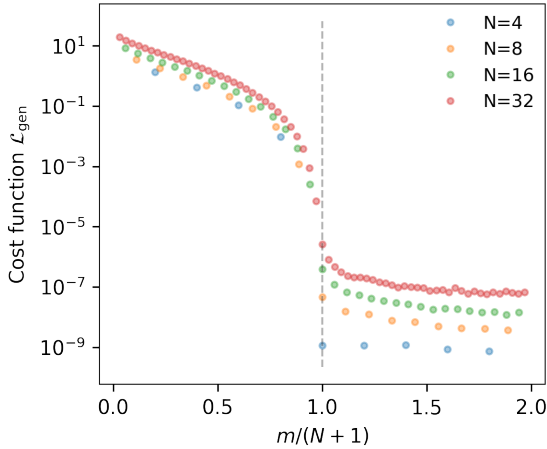


FIG. 7: Median value of the cost function  $\mathcal{L}_{\text{gen}}$  after 64 optimization trials, shows as a function of  $m/(N+1)$  for  $N = 4, 8, 16, 32$ .

also minimize  $\|Q(\mathbf{p}) - P\|_{\text{max}}$ . Therefore, the same cost function is used as in the exact configuration. For the

configuration of an  $N \times N$  matrix, the MPLC architecture with  $2N$  ports and the BE scheme are employed. The optimization algorithm is same as that used for the exact synthesis with the BE scheme, as described in Sec. III C.

We evaluate the approximation ability of the given linear converter by estimating the distribution of  $\|Q(\mathbf{p}) - P\|_{\text{max}}$  and calculating its 99th percentile. Assuming that errors in each matrix element are independent and identically distributed (i.i.d.), we apply extreme value statistics theory. This assumption is reasonable because the matrix to be realized is embedded in a unitary matrix, with no special basis vectors. The maximum of a sequence of i.i.d. variables follows the Generalized Extreme Value (GEV) distribution, a fact widely applied in fields such as risk analysis and rare event modeling [67, 68]. For evaluation, we consider the sequence of errors in matrix elements, where  $\|Q(\mathbf{p}) - P\|_{\text{max}}$  is expected to follow the GEV distribution due to the i.i.d. assumption across  $N^2$  matrix elements. To estimate this distribution, we run 512 optimization trials, varying the initial parameters, with each trial yielding one sample of  $\|Q(\mathbf{p}) - P\|_{\text{max}}$ . The distribution is then estimated

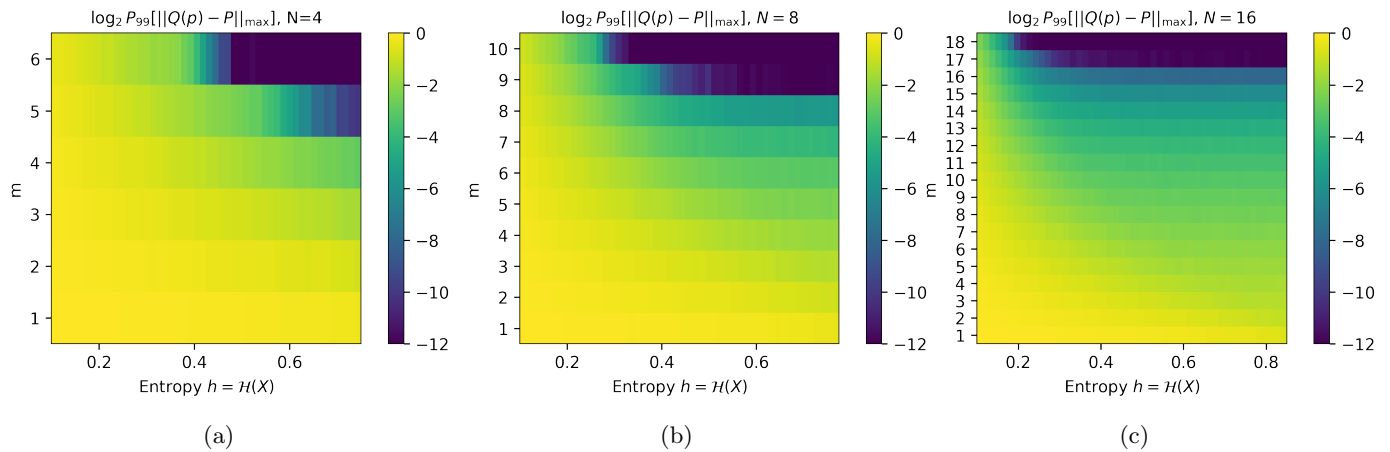


FIG. 8: The 99th percentile of the maximum error,  $\log_2 P_{99}[\|Q(\mathbf{p}) - P\|_{\max}]$ , in the synthesized approximate linear converter for  $N = 4$ ,  $N = 8$ , and  $N = 16$ . For each layer number  $m$  and entropy  $h$ , 512 optimization trials are conducted, and the 99th percentile of the maximum error is estimated using the GEV distribution.

using maximum likelihood estimation (MLE) based on the 512 samples, with its initial parameters derived via the probability-weighted moments method [69]. From the fitted distribution, the 99th percentile of the maximum error is calculated. In each optimization trial, the target matrix  $P$  and the mode mixers  $A_i$  are randomly sampled. To ensure the validity of fitting the GEV distribution and estimating its 99th percentile, we assess the goodness-of-fit using the Kolmogorov-Smirnov test [70, 71]. In all cases where the converter functions as an approximate converter, the null hypothesis that the observed samples originate from the GEV distribution cannot be rejected at the 5% significance level. In contrast, when the converter is exactly configured, the null hypothesis is rejected. This is because the assumption of i.i.d. no longer holds, as the error becomes limited by numerical precision during the optimization.

## B. Results

Figure 8 shows the 99th percentile of the maximum norm,  $P_{99}[\|Q(\mathbf{p}) - P\|_{\max}]$ , as a function of the number of layers  $m$  and the entropy of matrix  $\mathcal{H}(X)$ , for  $N = 4$ ,  $N = 8$ , and  $N = 16$ . For  $m \geq N + 1$ , the norm decreases significantly, consistent with the results shown in Fig. 7. Similar to the result in Fig. 5, the reduction of the maximum norm saturates when the entropy exceeds a certain threshold. For  $m < N + 1$ , where the number of layers is insufficient, the results indicate that the converter operates as an approximate converter, achieving matrices with errors dependent on both the number of layers and the entropy of the mixers. This implies that the converter can serve as an approximate converter within a defined maximum tolerable error. Increasing  $m$  leads to a reduction in the 99th percentile of the maximum norm for a fixed entropy. Comparing different  $N$ , fewer layers

$m$  are required to achieve the same accuracy for larger  $N$ , highlighting the scaling advantage of the approximate converter.

To further explore the scaling properties of the approximate converter, we determined the minimum number of phase shifters,  $mN$ , required to achieve a specified upper bound on the maximum norm. Figure 9 illustrates the least number of phase shifters  $mN$  needed to keep  $P_{99}$  below a given tolerable error. The red solid line corresponds to  $m = N + 1$ , representing exact synthesis of the linear converter, while markers denote the approximate converter. For each error bound, we evaluated approximate converters with Haar-randomly sampled mixers and those using low-entropy mixers ( $h = 0.4$ ). The approximate converter requires significantly fewer phase shifters than the exact converter. For  $N = 32$ , the number of phase shifters is reduced by more than 95% when allowing an error of  $P_{99} < 0.5$ . The use of low-entropy mixers increases the required number of phase shifters compared to the Haar-random case, though the difference becomes smaller as the error tolerance decreases. In some cases, low-entropy mixers with small  $N$  cannot satisfy the given error bounds, specifically for  $P_{99} < 0.1$  when  $N = 4$  or  $N = 6$ , and for  $P_{99} < 0.3$  when  $N = 4$ . Note that the figure is presented on a double-logarithmic scale, with exact synthesis requiring  $mN = (N + 1)N = O(N^2)$  phase shifters. In contrast, the approximate converter exhibits sub-quadratic scaling, as its slope is less steep than the red solid line. The greater the tolerated error, the more gradual the scaling becomes, indicating the scaling advantage of the approximate converter.

## V. CONCLUSION

We proposed an approximate linear converter based on MPLC for realizing a configurable and compact matrix-



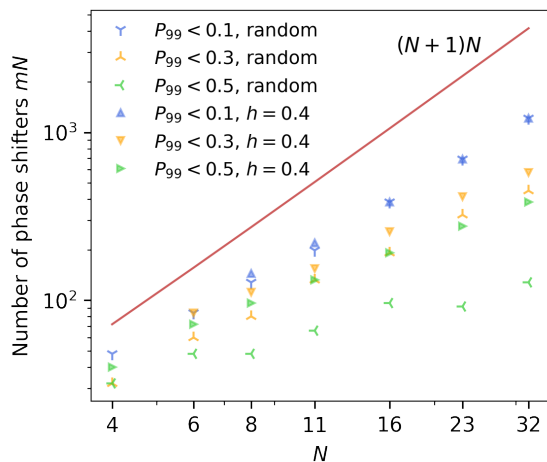


FIG. 9: Scaling of the number of phase shifters for the exact and approximate converters. The red solid line shows the case of  $m = N + 1$ , corresponding to the exact synthesis.

vector multiplication device. Our numerical results demonstrate that permitting errors in the converter’s synthesis enables sub-quadratic scaling in the number of phase shifters, a significant improvement over the  $O(N^2)$  scaling required for exact synthesis. We introduced Shannon matrix entropy as a metric for mode mixing capability and showed that the entropy of mixers can be reduced without compromising the universality or increas-

ing the approximation error. Additionally, we analyzed the structure of general linear converters composed of unitary converters and numerically demonstrated that the BE scheme outperforms the SVD scheme in iterative configuration. We believe this approach will facilitate scalable implementations of optical linear converters and advance the field of approximate computing using optics.

#### Appendix A: Degrees of freedom of the matrix root in Eq. 9

We present a proof for the unitary degrees of freedom of  $\sqrt{I - QQ^\dagger}$  in Eq. 9, where  $Q$  is a general matrix with singular value is less than or equal to 1. This proof also applies to  $\sqrt{I - Q^\dagger Q}$ . First, we show that  $I - QQ^\dagger$  is a positive semi-definite matrix. The singular value decomposition of  $Q$  is given by  $Q = W_1 D W_2$ , where  $W_1$  and  $W_2$  are unitary matrices, and  $D$  is a diagonal matrix with diagonal elements  $0 \leq \sigma_i \leq 1$ . The term inside the square root can be expressed as  $I - QQ^\dagger = I - (W_1 D W_2)(W_2^\dagger D W_1^\dagger) = W_1(I - D^2)W_1^\dagger$ . Since  $0 \leq \sigma_i \leq 1$ , all diagonal elements of  $I - D^2$  are non-negative. As a result, the matrix  $W_1(I - D^2)W_1^\dagger = W_1(I - D^2)W_1^{-1}$  represents a diagonalization with eigenvalues that are all greater than or equal to zero, meaning that the matrix is positive semi-definite. Since the square-root of a positive semi-definite matrix has unitary degree of freedom [72], we conclude that  $\sqrt{I - QQ^\dagger}$  has unitary degrees of freedom.

- 
- [1] Y. Shen, N. C. Harris, S. Skirlo, M. Prabhu, T. Baehr-Jones, M. Hochberg, X. Sun, S. Zhao, H. Larochelle, D. Englund, and M. Soljačić, Deep learning with coherent nanophotonic circuits, *Nature Photonics* **11**, 441 (2017).
  - [2] Y. Zuo, B. Li, Y. Zhao, Y. Jiang, Y.-C. Chen, P. Chen, G.-B. Jo, J. Liu, and S. Du, All-optical neural network with nonlinear activation functions, *Optica* **6**, 1132 (2019).
  - [3] M. Miscuglio, Z. Hu, S. Li, J. K. George, R. Capanna, H. Dalir, P. M. Bardet, P. Gupta, and V. J. Sorger, Massively parallel amplitude-only fourier neural network, *Optica* **7**, 1812 (2020).
  - [4] A. Ryou, J. Whitehead, M. Zhelyeznyakov, P. Anderson, C. Keskin, M. Bajcsy, and A. Majumdar, Free-space optical neural network based on thermal atomic nonlinearity, *Photon. Res.* **9**, B128 (2021).
  - [5] H. Zhang, M. Gu, X. D. Jiang, J. Thompson, H. Cai, S. Paesani, R. Santagati, A. Laing, Y. Zhang, M. H. Yung, Y. Z. Shi, F. K. Muhammad, G. Q. Lo, X. S. Luo, B. Dong, D. L. Kwong, L. C. Kwek, and A. Q. Liu, An optical neural chip for implementing complex-valued neural network, *Nature Communications* **12**, 457 (2021).
  - [6] M. S. S. Rahman, X. Yang, J. Li, B. Bai, and A. Ozcan, Universal linear intensity transformations using spatially incoherent diffractive processors, *Light: Science & Applications* **12**, 195 (2023).
  - [7] T. Zhou, W. Wu, J. Zhang, S. Yu, and L. Fang, Ultrafast dynamic machine vision with spatiotemporal photonic computing, *Science Advances* **9**, eadg4391 (2023), <https://www.science.org/doi/pdf/10.1126/sciadv.adg4391>.
  - [8] X. Tan, H. Song, Y. Ji, H. Tang, Y.-Y. Fang, X.-Y. Xu, Y.-Y. Li, X.-K. Li, K.-D. Zhu, and X.-M. Jin, Scalable and programmable three-dimensional photonic processor, *Phys. Rev. Appl.* **20**, 044041 (2023).
  - [9] T. Xu, W. Zhang, J. Zhang, Z. Luo, Q. Xiao, B. Wang, M. Luo, X. Xu, B. J. Shastri, P. R. Prucnal, and C. Huang, Control-free and efficient integrated photonic neural networks via hardware-aware training and pruning, *Optica* **11**, 1039 (2024).
  - [10] S. Bandyopadhyay, A. Sludds, S. Krastanov, R. Hamerly, N. Harris, D. Bunandar, M. Streshinsky, M. Hochberg, and D. Englund, Single-chip photonic deep neural network with forward-only training, *Nature Photonics* **18**, 1335 (2024).
  - [11] J. Feldmann, N. Youngblood, M. Karpov, H. Gehring, X. Li, M. Stappers, M. Le Gallo, X. Fu, A. Lukashchuk, A. S. Raja, J. Liu, C. D. Wright, A. Sebastian, T. J. Kippenberg, W. H. P. Pernice, and H. Bhaskaran, Parallel convolutional processing using an integrated photonic tensor core, *Nature* **589**, 52 (2021).
  - [12] Z. Guo, A. N. Tait, B. A. Marquez, M. Filipovich, H. Morison, P. R. Prucnal, L. Chrostowski, S. Shekhar,

- and B. J. Shastri, Multi-level encoding and decoding in a scalable photonic tensor processor with a photonic general matrix multiply (gemm) compiler, *IEEE Journal of Selected Topics in Quantum Electronics* **28**, 1 (2022).
- [13] C. M. Valensise, I. Grecco, D. Pierangeli, and C. Conti, Large-scale photonic natural language processing, *Photon. Res.* **10**, 2846 (2022).
- [14] M. Nakajima, K. Tanaka, K. Inoue, K. Nakajima, and T. Hashimoto, Densely parallelized photonic tensor processor on hybrid waveguide/free-space-optics, in *2023 International Conference on Photonics in Switching and Computing (PSC) (2023)* pp. 1–3.
- [15] M. Y.-S. Fang, S. Manipatruni, C. Wierzynski, A. Khosrowshahi, and M. R. DeWeese, Design of optical neural networks with component imprecisions, *Opt. Express* **27**, 14009 (2019).
- [16] R. Tang, R. Tanomura, T. Tanemura, and Y. Nakano, Lower-depth programmable linear optical processors, *Phys. Rev. Appl.* **21**, 014054 (2024).
- [17] S. A. Fldzhyan, M. Y. Saygin, and S. S. Straupe, Low-depth, compact, and error-tolerant photonic matrix-vector multiplication beyond the unitary group, *Opt. Express* **32**, 46239 (2024).
- [18] A. Ribeiro, S. Declercq, U. Khan, M. Wang, L. V. Iseghem, and W. Bogaerts, Column-row addressing of thermo-optic phase shifters for controlling large silicon photonic circuits, *IEEE Journal of Selected Topics in Quantum Electronics* **26**, 1 (2020).
- [19] B. V. Gurses, R. Fatemi, A. Khachaturian, and A. Hajimiri, Large-scale crosstalk-corrected thermo-optic phase shifter arrays in silicon photonics, *IEEE Journal of Selected Topics in Quantum Electronics* **28**, 1 (2022).
- [20] M. Miscuglio and V. J. Sorger, Photonic tensor cores for machine learning, *Applied Physics Reviews* **7**, 031404 (2020).
- [21] X. Li, N. Youngblood, W. Zhou, J. Feldmann, J. Swett, S. Aggarwal, A. Sebastian, C. D. Wright, W. Pernice, and H. Bhaskaran, On-chip phase change optical matrix multiplication core, in *2020 IEEE International Electron Devices Meeting (IEDM) (2020)* pp. 7.5.1–7.5.4.
- [22] Y. Miyatake, R. Tang, K. Makino, J. Tominaga, N. Miyata, M. Okano, K. Toprasertpong, S. Takagi, and M. Takenaka, Photonic matrix-vector multiplication with low-insertion-loss and non-volatile ge<sub>2</sub>sb<sub>2</sub>te<sub>3</sub>s<sub>2</sub> intensity modulators, *Journal of Lightwave Technology* **42**, 4347 (2024).
- [23] L. Yang, R. Ji, L. Zhang, J. Ding, and Q. Xu, On-chip cmos-compatible optical signal processor, *Opt. Express* **20**, 13560 (2012).
- [24] T. Ishihara, J. Shiomi, N. Hattori, Y. Masuda, A. Shinya, and M. Notomi, An optical neural network architecture based on highly parallelized wdm-multiplier-accumulator, in *2019 IEEE/ACM Workshop on Photonics-Optics Technology Oriented Networking, Information and Computing Systems (PHOTONICS) (2019)* pp. 15–21.
- [25] F. Brücknerhoff-Plückelmann, J. Feldmann, H. Gehring, W. Zhou, C. D. Wright, H. Bhaskaran, and W. Pernice, Broadband photonic tensor core with integrated ultra-low crosstalk wavelength multiplexers, *Nanophotonics* **11**, 4063 (2022).
- [26] H. Zhang, J. Thompson, M. Gu, X. D. Jiang, H. Cai, P. Y. Liu, Y. Shi, Y. Zhang, M. F. Karim, G. Q. Lo, X. Luo, B. Dong, L. C. Kwok, and A. Q. Liu, Efficient on-chip training of optical neural networks using genetic algorithm, *ACS Photonics* **8**, 1662 (2021).
- [27] M. Moralis-Pegios, G. Mourgias-Alexandris, A. Tsakyridis, G. Giamougiannis, A. Totovic, G. Dabos, N. Passalis, M. Kirtas, T. Rutirawut, F. Y. Gardes, A. Tefas, and N. Pleros, Neuromorphic silicon photonics and hardware-aware deep learning for high-speed inference, *Journal of Lightwave Technology* **40**, 3243 (2022).
- [28] G. Cong, N. Yamamoto, T. Inoue, Y. Maegami, M. Ohno, S. Kita, S. Namiki, and K. Yamada, On-chip bacterial foraging training in silicon photonic circuits for projection-enabled nonlinear classification, *Nature Communications* **13**, 3261 (2022).
- [29] S. Bandyopadhyay, A. Sludds, S. Krastanov, R. Hamerly, N. Harris, D. Bunandar, M. Streshinsky, M. Hochberg, and D. Englund, Single chip photonic deep neural network with accelerated training, *arXiv e-prints*, arXiv:2208.01623 (2022), arXiv:2208.01623 [cs.ET].
- [30] M. Courbariaux, Y. Bengio, and J.-P. David, Binaryconnect: Training deep neural networks with binary weights during propagations, in *Advances in Neural Information Processing Systems*, Vol. 28, edited by C. Cortes, N. Lawrence, D. Lee, M. Sugiyama, and R. Garnett (Curran Associates, Inc., 2015).
- [31] A. Polino, R. Pascanu, and D. Alistarh, Model compression via distillation and quantization, in *International Conference on Learning Representations (2018)*.
- [32] O. Zafrir, G. Boudoukh, P. Izsak, and M. Wasserblat, Q8bert: Quantized 8bit bert, in *2019 Fifth Workshop on Energy Efficient Machine Learning and Cognitive Computing - NeurIPS Edition (EMC2-NIPS) (2019)* pp. 36–39.
- [33] N. Burgess, J. Milanovic, N. Stephens, K. Monachopoulos, and D. Mansell, Bfloat16 processing for neural networks, in *2019 IEEE 26th Symposium on Computer Arithmetic (ARITH) (2019)* pp. 88–91.
- [34] J. Chee, Y. Cai, V. Kuleshov, and C. D. Sa, QuIP: 2-bit quantization of large language models with guarantees, in *Thirty-seventh Conference on Neural Information Processing Systems (2023)*.
- [35] E. Frantar, S. Ashkboos, T. Hoeffler, and D. Alistarh, OPTQ: Accurate quantization for generative pre-trained transformers, in *The Eleventh International Conference on Learning Representations (2023)*.
- [36] Y. Xu, X. Han, Z. Yang, S. Wang, Q. Zhu, Z. Liu, W. Liu, and W. Che, Onebit: Towards extremely low-bit large language models, in *The Thirty-eighth Annual Conference on Neural Information Processing Systems (2024)*.
- [37] J.-F. Morizur, L. Nicholls, P. Jian, S. Armstrong, N. Treps, B. Hage, M. Hsu, W. Bowen, J. Janousek, and H.-A. Bachor, Programmable unitary spatial mode manipulation, *J. Opt. Soc. Am. A* **27**, 2524 (2010).
- [38] G. Labroille, B. Denolle, P. Jian, P. Genevieux, N. Treps, and J.-F. Morizur, Efficient and mode selective spatial mode multiplexer based on multi-plane light conversion, *Opt. Express* **22**, 15599 (2014).
- [39] R. Tang, T. Tanemura, S. Ghosh, K. Suzuki, K. Tanizawa, K. Ikeda, H. Kawashima, and Y. Nakano, Reconfigurable all-optical on-chip mimo three-mode demultiplexing based on multi-plane light conversion, *Opt. Lett.* **43**, 1798 (2018).
- [40] N. K. Fontaine, R. Ryf, H. Chen, D. T. Neilson, K. Kim, and J. Carpenter, Laguerre-gaussian mode sorter, *Nature*

- Communications **10**, 1865 (2019).
- [41] S. Kuzmin, I. Dyakonov, and S. Kulik, Architecture agnostic algorithm for reconfigurable optical interferometer programming, *Opt. Express* **29**, 38429 (2021).
- [42] B. Bantysh, K. Katamadze, A. Chernyavskiy, and Y. Bogdanov, Fast reconstruction of programmable integrated interferometers, *Opt. Express* **31**, 16729 (2023).
- [43] Y. Taguchi, Y. Wang, R. Tanomura, T. Tanemura, and Y. Ozeki, Iterative configuration of programmable unitary converter based on few-layer redundant multiplane light conversion, *Phys. Rev. Appl.* **19**, 054002 (2023).
- [44] R. Tanomura, R. Tang, T. Tanemura, and Y. Nakano, Integrated inp optical unitary converter with compact half-integer multimode interferometers, *Opt. Express* **29**, 43414 (2021).
- [45] R. Tanomura, Y. Taguchi, R. Tang, T. Tanemura, and Y. Nakano, Entropy of mode mixers for optical unitary converter based on multi-plane light conversion, in *2022 Conference on Lasers and Electro-Optics Pacific Rim (CLEO-PR)* (2022) pp. 1–2.
- [46] K. Zelaya, M. Markowitz, and M.-A. Miri, The goldilocks principle of learning unitaries by interlacing fixed operators with programmable phase shifters on a photonic chip, *Scientific Reports* **14**, 10950 (2024).
- [47] K. Życzkowski, M. Kus, W. Słomczyński, and H.-J. Sommers, Random unistochastic matrices, *Journal of Physics A: Mathematical and General* **36**, 3425 (2003).
- [48] T. Kottos and U. Smilansky, Quantum chaos on graphs, *Phys. Rev. Lett.* **79**, 4794 (1997).
- [49] G. Tanner, Unitary-stochastic matrix ensembles and spectral statistics, *Journal of Physics A: Mathematical and General* **34**, 8485 (2001).
- [50] S. Gnutzmann and A. Altland, Spectral correlations of individual quantum graphs, *Phys. Rev. E* **72**, 056215 (2005).
- [51] S. S. Ion Nechita and M. Weber, Sinkhorn algorithm for quantum permutation groups, *Experimental Mathematics* **32**, 156 (2023), <https://doi.org/10.1080/10586458.2021.1926005>.
- [52] K. Arasu and M. T. Mohan, Entropy of orthogonal matrices and minimum distance orthostochastic matrices from the uniform van der waerden matrices, *Discrete Optimization* **31**, 115 (2019).
- [53] I. Bengtsson, Å. Ericsson, M. Kuś, W. Tadej, and K. Życzkowski, Birkhoff’s polytope and unistochastic matrices,  $n = 3$  and  $n = 4$ , *Communications in Mathematical Physics* **259**, 307 (2005).
- [54] P. Calabrese and J. Cardy, Evolution of entanglement entropy in one-dimensional systems, *Journal of Statistical Mechanics: Theory and Experiment* **2005**, P04010 (2005).
- [55] K. Kaneko, E. Iyoda, and T. Sagawa, Saturation of entropy production in quantum many-body systems, *Phys. Rev. E* **96**, 062148 (2017).
- [56] Y. Fuji and Y. Ashida, Measurement-induced quantum criticality under continuous monitoring, *Phys. Rev. B* **102**, 054302 (2020).
- [57] R. Tanomura, R. Tang, T. Umezaki, G. Soma, T. Tanemura, and Y. Nakano, Scalable and robust photonic integrated unitary converter based on multiplane light conversion, *Phys. Rev. Appl.* **17**, 024071 (2022).
- [58] M. Markowitz, K. Zelaya, and M.-A. Miri, Auto-calibrating universal programmable photonic circuits: hardware error-correction and defect resilience, *Opt. Express* **31**, 37673 (2023).
- [59] Y. Taguchi, Y. Wang, R. Tanomura, T. Tanemura, and Y. Ozeki, Rapidly convergent fabrication-error-tolerant unitary processor using few-layer-redundant multi-plane light conversion, in *Conference on Lasers and Electro-Optics/Europe (CLEOEurope) 2023* (Optica Publishing Group, 2023) pp. JSIII–4.2.
- [60] M. Y. Saygin, I. V. Kondratyev, I. V. Dyakonov, S. A. Mironov, S. S. Straupe, and S. P. Kulik, Robust architecture for programmable universal unitaries, *Phys. Rev. Lett.* **124**, 010501 (2020).
- [61] R. Tanomura, R. Tang, T. Tanemura, and Y. Nakano, Demonstration of error-tolerant integrated optical processors based on multi-plane light conversion, *IEEE Photonics Technology Letters* **35**, 1275 (2023).
- [62] P. Virtanen, R. Gommers, T. E. Oliphant, M. Haberland, T. Reddy, D. Cournapeau, E. Burovski, P. Peterson, W. Weckesser, J. Bright, S. J. van der Walt, M. Brett, J. Wilson, K. J. Millman, N. Mayorov, A. R. J. Nelson, E. Jones, R. Kern, E. Larson, C. J. Carey, Í. Polat, Y. Feng, E. W. Moore, J. VanderPlas, D. Laxalde, J. Perktold, R. Cimrman, I. Henriksen, E. A. Quintero, C. R. Harris, A. M. Archibald, A. H. Ribeiro, F. Pedregosa, P. van Mulbregt, and SciPy 1.0 Contributors, SciPy 1.0: Fundamental algorithms for scientific computing in Python, *Nature Methods* **17**, 261 (2020).
- [63] R. Fletcher, *Practical Methods of Optimization*, 2nd ed. (John Wiley & Sons, New York, NY, USA, 1987).
- [64] Y. Taguchi and Y. Ozeki, Standalone gradient measurement of matrix norm for programmable unitary converters, *J. Opt. Soc. Am. B* **41**, 1425 (2024).
- [65] A. Gilyén, Y. Su, G. H. Low, and N. Wiebe, Quantum singular value transformation and beyond: exponential improvements for quantum matrix arithmetics, in *Proceedings of the 51st Annual ACM SIGACT Symposium on Theory of Computing*, STOC 2019 (Association for Computing Machinery, New York, NY, USA, 2019) p. 193–204.
- [66] D. Camps, L. Lin, R. Van Beeumen, and C. Yang, Explicit quantum circuits for block encodings of certain sparse matrices, *SIAM Journal on Matrix Analysis and Applications* **45**, 801 (2024).
- [67] R. A. Fisher and L. H. C. Tippett, Limiting forms of the frequency distribution of the largest or smallest member of a sample, *Mathematical Proceedings of the Cambridge Philosophical Society* **24**, 180–190 (1928).
- [68] B. Gnedenko, Sur la distribution limite du terme maximum d’une série aléatoire, *Annals of Mathematics* **44**, 423 (1943).
- [69] J. R. M. Hosking, J. R. Wallis, and E. F. Wood, Estimation of the generalized extreme-value distribution by the method of probability-weighted moments, *Technometrics* **27**, 251 (1985).
- [70] K. A. L., Sulla determinazione empirica di una legge di distribuzione, *G. Ist. Ital. Attuari* **4**, 83 (1933).
- [71] N. Smirnov, Table for Estimating the Goodness of Fit of Empirical Distributions, *The Annals of Mathematical Statistics* **19**, 279 (1948).
- [72] A. Antoniou and W.-S. Lu, Basics of linear algebra, in *Practical Optimization: Algorithms and Engineering Applications* (Springer US, New York, NY, 2021) pp. 635–688.